Disentangling the ligand and electronic structure in KVPO4F1-xOx positive electrode materials by Valence-to-Core X-ray emission spectroscopy

Jazer Jose H. Togonon, Antonella Iadecola, Romain Wernert, Kriti Choudhary, Mauro Rovezzi, Jean-Noël Chotard, Lorenzo Stievano, Alessandro Longo, Laurence Croguennec

Disentangling the ligand and electronic structure in $KVPO_4F_{1-x}O_x$ positive electrode materials by Valence-to-Core X-ray emission spectroscopy

Jazer Jose H. Togonon[1,2,3], Antonella Iadecola[4,5,*], Romain Wernert[2,4,6], Kriti Choudhary[3,4,7], Mauro Rovezzi[8], Jean-Noël Chotard[3,4,7], Lorenzo Stievano[3,4,6], Alessandro Longo[9,10,*], Laurence Croguennec[2,3,4,*]

Authors' Address

[1] Synchrotron SOLEIL, L'Orme des Merisiers, Saint-Aubin, 91192 Gif-sur-Yvette, France
[2] Univ. Bordeaux, CNRS, Bordeaux INP, ICMCB, UMR 5026, F-33600 Pessac, France
[3] ALISTORE-ERI European Research Institute, FR CNRS 3104, F-80039 Amiens Cedex 1, France
[4] RS2E, Réseau Français sur le Stockage Electrochimique de l'Energie, FR CNRS #3459, Amiens F-80039 Cedex 1, France
[5] Sorbonne Université, PHysicochimie des Electrolytes, Nanosystèmes InterfaciauX (PHENIX), UMR CNRS 8234, 75252 Paris, France
[6] ICGM, Univ. Montpellier, CNRS, ENSCM, 34095 Montpellier, France
[7] Université de Picardie Jules Verne, Laboratoire de Réactivité et Chimie des Solides (LRCS), 15 rue Baudelocque, 80000, Amiens, France
[8] Univ. Grenoble Alpes, CNRS, IRD, Irstea, Météo France, OSUG, FAME, F-38000 Grenoble, France
[9] European Synchrotron Radiation Facility (ESRF), 71, Avenue des Martyrs, Grenoble F-38000, France
[10] Istituto per lo Studio dei Materiali Nanostrutturati (ISMN)-CNR, UOS Palermo, via Ugo La Malfa 153, Palermo 90146, Italy
*Corresponding authors: Antonella.iadecola@synchrotron-soleil.fr; alessandro.longo@esrf.fr, laurence.croguennec@icmcb.cnrs.fr

Keywords: Valence-to-Core X-ray emission spectroscopy, electronic structure, vanadium fluoride phosphate, vanadium oxide phosphate, vanadyl-type bond, potassium-ion battery, X-ray emission spectroscopy

ABSTRACT

Understanding the intricate crystal structure of polyanionic positive electrode materials is essential for elucidating the mechanisms involved during cycling and predicting the working potential of the electrode. To achieve this goal, a clear comprehension of how the coordination environment of the transition metal ion influences the ionicity/covalency of the metal-ligand bonds is necessary. Yet, discriminating these ligands poses challenges due to the limited sensitivity to light elements of common characterization techniques such as X-ray diffraction (XRD) and extended X-ray absorption fine structure (EXAFS) analysis. To address this issue, we employed valence-to-core Kβ X-ray emission spectroscopy combined with *ab initio* modelling and conducted a systematic investigation using potassium vanadium oxyfluoride phosphate compounds with the general formula $KVPO_4F_{1-x}O_x$ (x = 0, 0.25, 0.5, 0.75, 1). Our approach allows distinguishing the contributions of V-F, V-O, and V=O bonds at the Kβ" region, with intensities highly correlated to the F^- and O^{2-} anion composition. Additionally, the evolution of the features at the $K\beta_{2,5}$ region is highly correlated to the presence of short V=O bonds, strongly influencing the electrode potential of the material. Density of state (DOS) analysis based on *ab initio* modelling of the end member compounds $KVPO_4F$ and $KVOPO_4$ further supports the existence of V-F and V=O bonding through the mixing of F/O *p*-DOS with V *d*-DOS. Overall, we present a detailed and reliable approach for understanding the occupied electronic states of the bulk material, proving valuable for a thorough comprehension of the structure of positive electrode materials in batteries.

INTRODUCTION

Over the span of years, potassium ion batteries (KIBs) have become a possible alternative for energy storage applications. This is mainly driven by the high abundance of potassium, the low electrochemical voltage of K^+/K vs. NHE (normal hydrogen electrode) and the ability of K^+ ions to (de)intercalate into graphite negative electrodes as well as in a large panel of positive electrodes such as transition metal layered oxides and polyanionic materials – properties highly sought after for producing high-energy batteries. [1,2] The intercalation chemistry involved in K-ion batteries is similar to the rocking-chair mechanism of charge carrier ions, as seen in Li-on batteries. However, this technology is still at its early stage, and indeed research must be intensified in order to develop new positive and negative electrode materials, to formulate electrolytes to stabilize the electrode-electrolyte interfaces, and to address the struggle against irreversible reactions such as self-discharge and cross-talking between the electrodes. One promising class of positive electrodes for KIBs includes potassium vanadium fluoride phosphate ($KVPO_4F$) and potassium vanadium oxide phosphate ($KVOPO_4$), which offer a high theoretical capacity of 131 $mAh \cdot g^{-1}$ and an average working potential reaching above 4.30 V vs K^+/K. This results in a theoretical energy density of up to 560 $Wh \cdot kg^{-1}$. [3,4]

These polyanionic materials possess a $KTiOPO_4$-type structure, which is constructed of infinite chains of corner-sharing octahedra with two different vanadium sites, interconnected by PO_4 tetrahedra (Figure 1a). The structure can be represented by the general formula $KVPO_4X$ (X = F, O), where the anion X resides in VO_4X_2 octahedra in alternating *cis* and *trans* configurations (Figure 1b). The octahedra along the chains are linked through these corners which are occupied, either by fluorine forming a $V^{III}O_4F_2$ "ionic" entity, or by oxygen forming a $\{V^{IV}{=}O\}O_5$ entity with a highly "covalent" vanadyl-type bond $\{V{=}O\}^{2+}$.

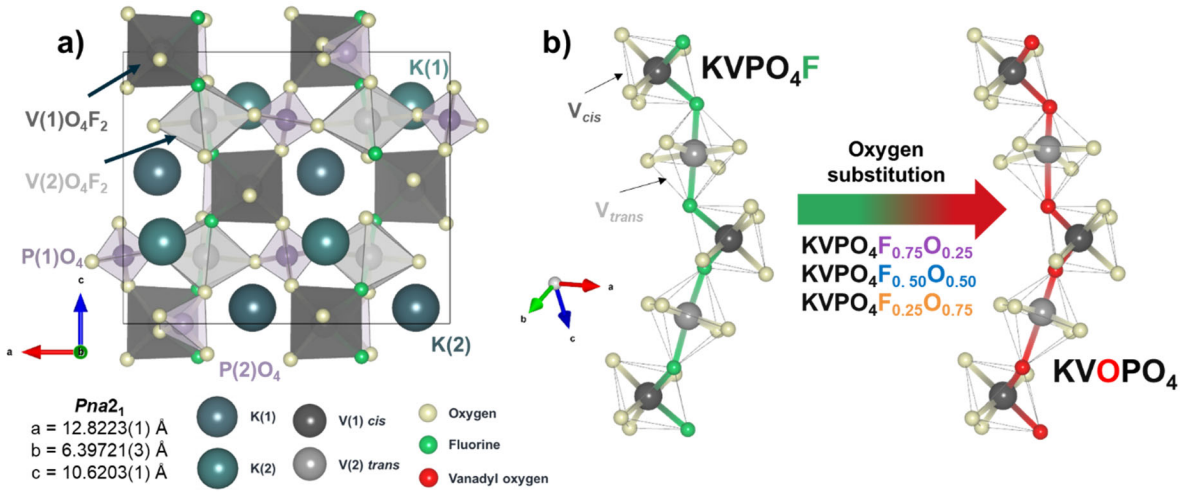

Figure 1. a) Crystal structure of $KVPO_4F$, and b) the alternating V_{cis} and V_{trans} octahedral environments bridged by F^- and O^{2-} ligands for $KVPO_4F$ and $KVOPO_4$, respectively.

Recent studies have shown that these anions play a significant role in the electrochemical properties and structural evolution of this type of vanadium-based polyanionic electrode materials, and not only in the case of KIBs. [5–8] Tavorite-type $LiVOPO_4$, for instance, was demonstrated to exhibit multielectron transfer properties wherein Li^+ can either be deintercalated to form $VOPO_4$ or intercalated to produce Li_2VOPO_4. These reactions trigger V^{5+}/V^{4+} or V^{4+}/V^{3+} redox couples for the former and the

latter, respectively. Distorted VO_6 octahedra with a V=O bonding scheme were observed in $V^{V}OPO_4$ and $LiV^{IV}OPO_4$ whereas vanadium lies in a symmetric octahedral coordination site in $Li_2V^{III}OPO_4$. [9] Another intriguing redox mechanism was observed in $Na_3V^{III}_2(PO_4)_2F_3$: the deintercalation of 2 Na^+ ions from the structure per formula unit leads to the formation of V^{5+} - V^{3+} pairs in the composition $Na_1V_2(PO_4)_2F_3$, and not as it could have been expected to V^{4+} - V^{4+}. [5,10,11] Such a wide range of redox mechanisms and evolutions in the local environment of vanadium are rather challenging to untangle. For these materials, it is thus critical to understand the local structural changes induced by variations in the ligand nature, considering especially that they affect the overall electronic structure and properties of the electrode material, in its pristine state and then upon cycling during the operation of the battery. [12,13] Indeed, intercalation reactions are of course highly dependent on the redox centers involved, and thus on the nature of the ligands present in the Vanadium environments. For these reasons, it is of primary importance to understand the spectroscopic markers that allow to distinguish all the phenomena involved in the charge compensation mechanisms in these mixed anion polyanionic electrode materials of interest for batteries.

Core level spectroscopies are commonly employed to study the chemical state and bonding, local geometry and dynamics in electron transfer processes at specific atomic species. [14] Among them, X-ray absorption spectroscopy (XAS) is the technique of choice to investigate the electronic structure and the local environment of the redox centers. A recent XAS study of a series of vanadium oxyfluoride phosphate compounds $KVPO_4F_{1-x}O_x$ (x = 0, 0.25, 0.5, 0.75, 1) [6] showed that the V K-edge position undergoes a linear shift towards higher energy, suggesting the evolution of the oxidation state of vanadium from V^{3+} to V^{4+} for, respectively, the x = 0 and x = 1 end members and partial oxidation states for intermediate compounds with fractional F/O content. [6,15,16] While additional information on the V local environment can be obtained from the analysis of the extended X-ray absorption fine structure (EXAFS), certain difficulties may arise as light elements are impossible to discriminate. Furthermore, while XANES pre-peak features could provide important insights on the V-F, V-O and V=O bonds contributing to the charge compensation involving the V 3*d* unoccupied states, [8,11,17] one main limitation is the lack of a quantitative deconvolution of these contributions due to the lack of selectivity toward F^- and O^{2-} anions. This means that complementary approaches must be used to obtain a full description of the vanadium sites and of their redox properties in addition to the information on the vanadium oxidation state and local environment provided by XAS.

Complementary to XAS, non-resonant hard X-ray emission spectroscopy (XES) is a suitable tool to probe the electronic structure of a material, with bulk sensitivity. [18,19] For 3*d* transition metals, such as vanadium, the Kβ XES spectrum is comprised of two main regions of interest: the Kβ Core-to-Core (CtC) and the Kβ Valence-to-Core (VtC) emission lines corresponding, respectively, to $3p \rightarrow 1s$ and ligand $2s/2p$ mixed with metal $3d \rightarrow 1s$ electric dipole transitions (Figure 2b). The former appears at lower energies ranging from approximately 5400 to 5435 eV, while the latter is detected at higher energies from the high energy tail of CtC XES and extends up to approximately 5470 eV (Figure 2a).

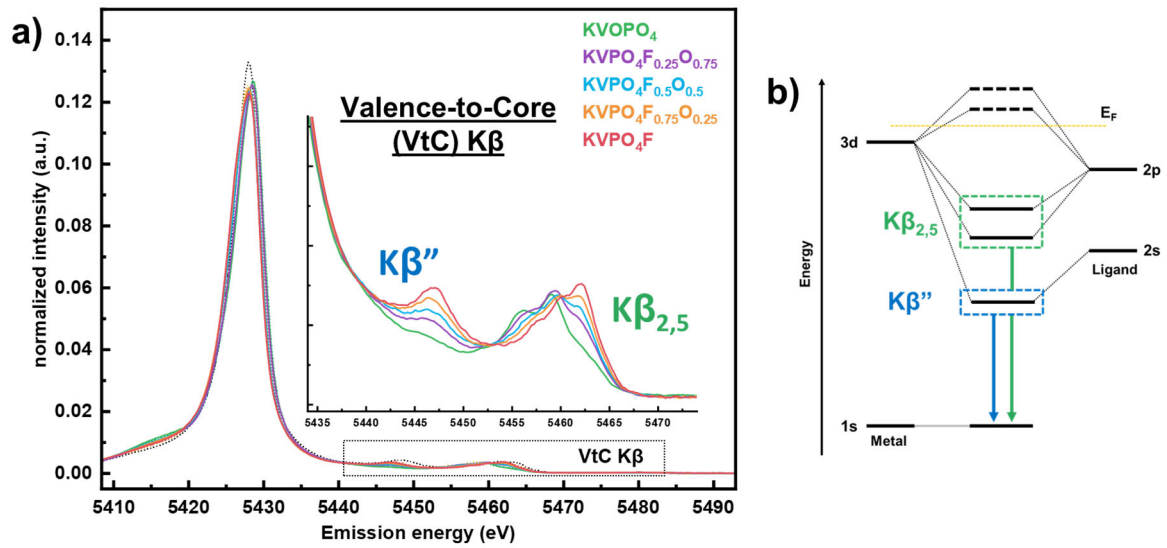

Figure 2. a) Full Kβ XES spectra of vanadium with inset showing the Kβ VtC region, and b) the corresponding electronic transitions of each emission line.

Kβ CtC XES has been already successfully used to characterize 3*d* transition metals. [18,20,21] This paper focuses more specifically on Kβ VtC XES, which arises from the relaxation of electrons in ligand-localized valence orbitals that fill the 1*s* core hole, emitting fluorescent photons in the process, primarily probing the filled, ligand-based orbitals of a metal complex. Although having the lowest transition probability (and thus the lowest intensity) due to its nature as a dipole-forbidden transition, significant information can be collected from the VtC XES. It has two distinct regions, Kβ" and $K\beta_{2,5}$, with Kβ" providing information on the n*s* orbital of the ligand to the *s* orbital of the metal through the crossover transition effects of electrons, while $K\beta_{2,5}$ offers additional information on the hybridization of *p*- and *d*- orbitals of the ligands and the metal, respectively. Hence, VtC XES directly probes the energy of the valence molecular orbital (MO) with respect to vanadium's 1*s* orbital. [19]

VtC XES was directly used to probe the energy of the valence MOs with respect to an absorber metal atom and was shown to be highly sensitive to ligand type [19,22–24], ligand orientation, [25] and local structure [26] in studies of both small and large molecules as well as biological catalysts, where the understanding of the molecular processes is highly critical. However, its application to the solid-state chemistry of energy storage materials remains scarce and insights from the VtC XES would complement the use of conventional X-ray spectroscopies for electrode materials.

To understand the impact of fluorine-oxygen composition in the $KVPO_4F$ - $KVOPO_4$ system, experimental VtC XES spectra of a family of mixed anion compositions ($KVPO_4F_{1-x}O_x$, x = 0, 0.25, 0.50, 0.75, 1) were analyzed. Our systematic approach in combining VtC XES and *ab initio* calculations provides a comprehensive analytical tool for evaluating the complex electronic structures of occupied states close to the Fermi level, which governs the electrochemical properties of these materials as positive electrodes for KIBs. In addition, this paper highlights the importance of establishing a strong correlation between measurable quantities using a multimodal approach to elicit a robust interpretation of the intricate electronic structures, particularly in compounds with covalent vanadyl-type environments.

MATERIALS AND METHODS

Sample preparation

Five different $KVPO_4F_{1-x}O_x$ (x = 0, 0.25, 0.5, 0.75, 1) compositions were prepared by solid-state high-temperature synthesis in a controlled argon atmosphere as described in detail in a previous article. [6] Structural and purity analyses of the compounds were previously performed and described in detail in a previous work. [6]

Vanadium Kβ X-ray emission spectroscopy (XES)

Pure samples were made into pellets of 5 mm in diameter. No Kapton films were used since the compounds are stable in air and ambient conditions. XES data were collected at beamlines BM16 [27] and ID20 of the European Synchrotron Radiation Facility (ESRF). The full Kβ XES emission lines were measured at both beamlines to ensure reproducibility of the results. VtC Kβ measurements are compared and shown in Figure S1 to show reproducibility. Data analysis was performed using the spectra obtained at ID20.

At the ID20, the whole span of the Kβ emission line was measured covering both CtC Kβ (5380 – 5430 eV) and VtC Kβ region (5430 - 5470 eV). The measurement was done using a Von Hamos spectrometer equipped with three cylindrically bent Si (440) crystal analyzer with bending radius of R = 250 mm and an incident energy of 9.7 keV. [28] The total integration time for each scan was approximately 15 mins and the data were recorded simultaneously by three different detectors. Individual scans were first averaged using the PyMCA [29] software package. All spectra were background-subtracted and were normalized with respect to the integrated sum of the full range of the Kβ XES. A spline-type baseline for the Kβ VtC region was created using Fityk [30] (Figure S2) to obtain baseline-subtracted flat spectra, for easier comparison with theoretical results and feature identification. This was done using the high energy tail of the V Kβ CtC emission line (5430-5435 eV) up to the high energy end of the Kβ VtC region.

Theoretical calculations

The FDMNES code [31,32] was used to perform the *ab initio* calculations to simulate the V Kβ VtC XES spectra and obtain the electron densities of state (DOS) for $KVPO_4F$ and $KVOPO_4$. This code can model emission spectra within the one-particle potential approximation and treat large systems where correlation weakly affects the spectra. The crystallographic information of $KVPO_4F$ and $KVOPO_4$ obtained from a previous work [6] were used to describe their structure and the corresponding atomic positions. Multiple scattering theory based on the muffin-tin (MT) approximation was used for the potential shape of the Green scheme and nonrelativistic calculations were employed with self-consistent calculation features. [33] The MT radii were adjusted to ensure proper overlap between the different spherical potentials. A Gaussian convolution (1.0 eV) was used to account for core-hole lifetime, photoelectron state width, and experimental resolution. Finally, the obtained spectra were normalized to the same integrated intensity of the experimental data within the suitable emission energy range. Input files are available in the supplementary information section of the article (Table S1 and Table S2 for $KVPO_4F$ and $KVOPO_4$, respectively).

RESULTS AND DISCUSSION

All $KVPO_4F_{1-x}O_x$ samples have an orthorhombic symmetry structure described within the *Pna*2_1 space group. Structural analysis using Rietveld refinement of the XRD patterns in our earlier work [6] revealed a single phase in all materials with no segregation into end-member compounds. This indicates a statistical distribution of F^- and O^{2-} bridging atoms throughout the crystal structure. [6,15] For partially substituted materials, bond lengths obtained from XRD pattern refinements are the average of different chemical configurations. The vanadium atoms occupy two symmetrically inequivalent sites existing in octahedral coordination, forming chains connected by either F or O atoms arranged in alternating *cis*- and *trans*- configurations, as shown in Figure 1b. The chains grow along the [011] and [0$\bar{1}$1] directions. It is important to note that the local geometric structure of the vanadium sites has significant differences in bond lengths and is mainly driven by the ligand repositioning rather than the displacement of V within the octahedra. [6]

It was previously revealed by XAS that the average oxidation state of vanadium increases linearly as a function of oxygen content on going from $KV^{III}PO_4F$ to $KV^{IV}OPO_4$. [6,15] The bond valence sums (BVS), calculated using the parameters in Table S3 and from the XRD data, perfectly agree with the formal oxidation state of V obtained by XAS and were taken as close estimates of the formal oxidation states (Table 1).

Table 1. Refined structural parameters corresponding to the local structure of VO_4X_2 (X = O, F) octahedra of the full and partially substituted $KVPO_4F_{1-x}O_x$ and other reference materials [6,34]

Compound	x	Bonding type	Ligand composition in the octahedra	XRD obtained average V-X bond lengths, Å			Average Bond Valence Sum
				$(V_{cis}\text{-}X)_{ave}$	$(V_{trans}\text{-}X)_{ave}$	V-X_{ave}	
$KVPO_4F$	0	V-F	2	1.975(4)	1.993(4)	1.984(4)	3.03
		V-O	4				
$KVPO_4F_{0.75}O_{0.25}$	0.25	V-F	1.5	1.984(3)	2.001(3)	1.993(3)	3.25
		V-O	4.25				
		V=O	0.25	1.885(3)	1.908(3)	1.896(3)	
$KVPO_4F_{0.5}O_{0.5}$	0.5	V-F	1	1.985(4)	2.008(3)	1.997(3)	3.50
		V-O	4.5				
		V=O	0.5	1.822(2)	1.825(2)	1.823(2)	
$KVPO_4F_{0.25}O_{0.75}$	0.75	V-F	0.5	1.992(4)	2.035(4)	2.013(4)	3.74
		V-O	4.75				
		V=O	0.75	1.728(2)	1.735(2)	1.732(2)	
$KVOPO_4$	1	V-O	5	1.992(3)	2.040(5)	2.016(3)	3.96
		V=O	1	1.683(2)	1.666(2)	1.675(2)	
β-$VOPO_4$	-	V-O	5			2.024(7)	5.26
		V=O	1			1.565(8)	
$NaVOPO_4$	-	V-O	5			2.056(4)	3.90
		V=O	1			1.631(7)	
$NaV_2(PO_4)_3$	-	V-O	6			1.906(4)	4.32
$Na_3V_2(PO_4)_3$	-	V-O	6			1.992(7)	3.07

Ligand sensitivity of the Kβ" emission line in $KVPO_4F_{1-x}O_x$

As previously discussed, the Kβ VtC emission line can be divided into two main regions: the Kβ" and the $K\beta_{2,5}$. Both regions provide valuable information about the occupied electronic states at the valence band or the electronic structure near the Fermi level. Specifically, the peaks in the Kβ" region (5434 – 5451 eV) originate from the electronic transition from the 2*s* orbitals of fluorine and oxygen to the 1*s* orbital of vanadium through the "crossover" transition effects of electrons. In Figure 3a, two separate peaks at approximately ~5440 eV and ~5447 eV suggest the contribution from F^- and O^{2-} anions, respectively, as observed in the XES spectrum.

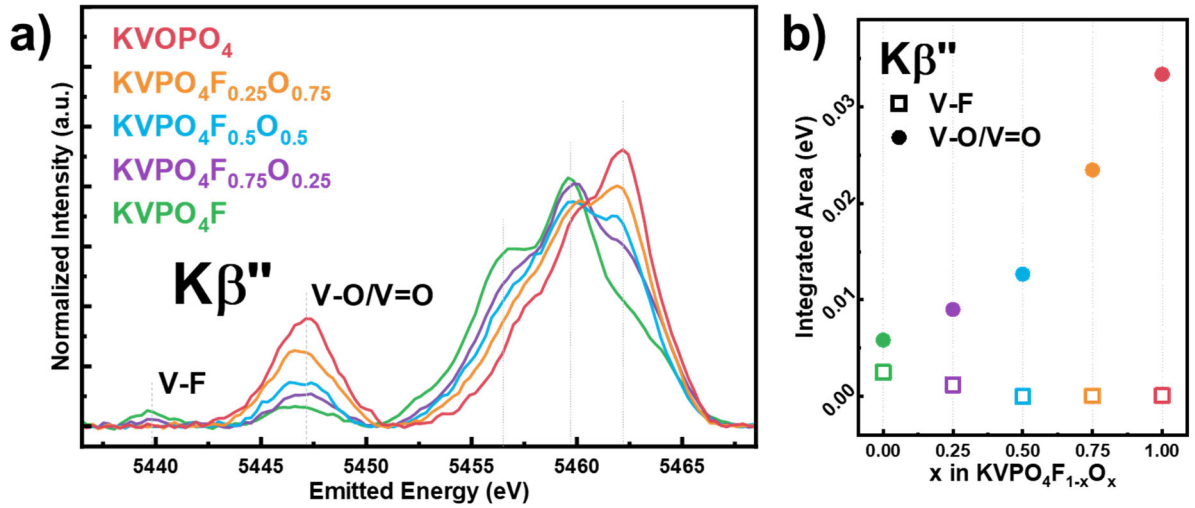

Figure 3. a) Normalized Kβ VtC XES emission lines of $KVPO_4F_{1-x}O_x$ (x = 0, 0.25, 0.5, 0.75, 1) and b) correlation between the composition and the integrated intensity at the Kβ" region.

In $KVPO_4F$, the faint peak visible at ~5440 eV decreases in intensity with the increase of the O content, and thus can be attributed to the presence of F in the compound series. This conclusion is further supported by the absence of such feature in non-fluorine-containing reference compounds such as $Na_3V_2(PO_3)_4$, $NaV_2(PO_3)_4$, $NaVOPO_4$, and $VOPO_4$, as shown in Figure 4a. On the other hand, the peak at ~5447 eV is observed in the spectra of all mixed anion compounds. Notably, it is observed that starting from $KVPO_4F$, its intensity increases, although not linearly, with the increase in O content in the $KVPO_4F_{1-x}O_x$ series (from four O atoms in the first coordination shell of V for $KVPO_4F$ to six O atoms for $KVOPO_4$), which is highly correlated to the modification of the iono-covalent character of the V-X bonds [7]. As previously discussed, the substitution of F^- with O^{2-} in the series leads to the formation of a highly covalent V=O bond, causing distortion in the octahedral environment of vanadium from a quasi O_h symmetry to a C_{4v} symmetry. This distortion in local geometry results in an increased intensity of the peak at ~5447 eV throughout the mixed polyanionic compound series as presented in Figure 3b, accompanied by a decrease in bond length at the V=O site (Table 1). This relationship becomes evident when comparing with reference materials such as $NaVOPO_4$ (V=O ~ 1.63 Å) and $VOPO_4$ (V=O ~ 1.57 Å), which exhibit further decreasing V=O bond length versus $KVOPO_4$ (V=O ~ 1.67 Å) and thus the increasing peak intensity at ~5447 eV (Figure 4a).

Local geometry sensitivity of $K\beta_{2,5}$ emission line in $KVPO_4F_{1-x}O_x$

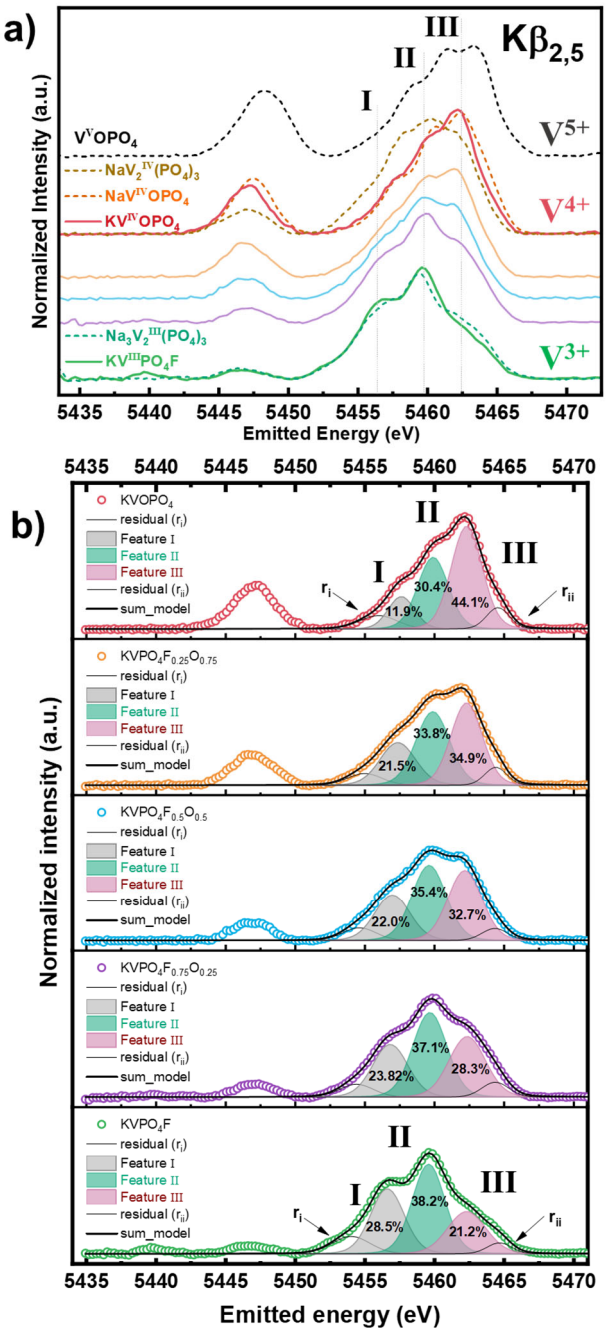

Figure 4. a) Normalized Kβ VtC XES emission lines of $KVPO_4F_{1-x}O_x$ (x = 0, 0.25, 0.5, 0.75, 1) with the corresponding reference materials (plotted in dashed lines) having different oxidation states and local geometries, and b) the experimental spectra (open circles) of the $KVPO_4F_{1-x}O_x$ along with the peak deconvolution using five Voigt functions (solid lines).

The $K\beta_{2,5}$ region provides information about the interaction between the 2*p* orbitals of fluorine and oxygen, and the 3*d* orbitals of vanadium, along with their corresponding electronic transitions to the 1*s* core hole of vanadium. In a first approximation, triple-peak features are observed for the series of potassium vanadium oxyfluoride phosphates which are denoted as I, II and III in the order of increasing emission energy (Figure 4a). This is consistent with a previous work reported on lithium vanadyl oxide

phosphate ($LiVOPO_4$). [22] In addition, an isosbestic point is observed in the series at approximately 5460 eV (Figure S3), indicating a correlation between features II and III. Moreover, it should be mentioned that the recorded spectra for the end members of the $KVPO_4F_{1-x}O_x$ series are sufficient to describe the general evolution of the $K\beta_{2,5}$ region for all the materials with intermediate compositions (x = 0.25, 0.50, 0.75), as their spectra can be obtained by the simple weighed linear combination of the spectra of the end members as shown in Table 2. The obtained results exhibit a high level of agreement with the expected F/O ratio, confirming precise control over the stoichiometry and indicating comparable local structures in both the end member compounds and the partially substituted phases. Similar results were obtained from the previously obtained XAS spectra, suggesting high similarity as to the extent of probing in the local structure. [6]

Table 2. Results from the linear combination fitting of the $K\beta_{2,5}$ VtC XES spectra of intermediate $KVPO_4F_{1-X}O_x$ calculated from the end member compounds $KVPO_4F$ and $KVOPO_4$

Compound	$KVPO_4F$ (%)	$KVOPO_4$ (%)	R factor
$KVPO_4F$	100	0	
$KVPO_4F_{0.75}O_{0.25}$	71	29	2.12×10^{-7}
$KVPO_4F_{0.50}O_{0.50}$	56	44	2.29×10^{-7}
$KVPO_4F_{0.25}O_{0.75}$	28	72	1.00×10^{-7}
$KVOPO_4$	0	100	

A more detailed comparison of spectral changes was carried out using a curve-fitting procedure of the experimental spectra employing five symmetric Voigt functions. [21] The goal of this approach is to provide a quantification to the individual contributions of the highlighted and defined features at the $K\beta_{2,5}$ region. The main features I, II, and III, enhanced in Figure 4b to clearly define the Gaussian/Lorentzian mixture of the projections, are accompanied by two less intense components with a similar shape, located at lower (r_i) and higher (r_{ii}) emission energies, respectively. These additional weak components are needed to adequately fit the spectra, and represent the small probabilities related to electronic transitions such as the hybridization effects of orbitals which are related to the degree of symmetry in the local geometry. A decreasing area for both features I (28.5% to 11.9 %) and II (38.2 % to 30.4 %), and an increasing area in feature III (21.2 % to 44.1 %) in the series are observed from $KVPO_4F$ to $KVOPO_4$, respectively as seen in Figure 4b and Figure S4a. The systematic evolution of the three features also correlates with the changes in the average bond length of the series of compounds containing both V-F and V=O bonds, as seen in Figure S4b. Overall, these parameters and observations substantiate the initial hypotheses concerning the evolution of the features as the composition of V-F and V=O varies for each contribution within the curve-fitted model (Table S4 and Figure S4).

To evaluate the correlation between the oxidation state of vanadium and its local environment, qualitative reference samples for V^{3+}, V^{4+}, and V^{5+} were used to compare the series of compounds (Figure 4a). Interestingly, two V^{4+} reference samples were employed – $NaVOPO_4$ with a vanadyl bond and $NaV_2(PO_4)_3$ without – to account for changes associated with both the formal oxidation state and the significant difference in bond iono-covalency that could impact the spectral features. For the comparison between the two compounds, the existence of a vanadyl bond in $NaVOPO_4$ led to a

substantial shift of the $K\beta_{2,5}$ spectral features towards higher emission energies compared to that of $NaV_2(PO_4)_3$. In the case of $KVOPO_4$ (V=O ~ 1.67 Å) which is also expected to contain V^{4+}, the observed spectrum resembles to that of $NaVOPO_4$ (V=O ~ 1.63 Å) and is substantially different from that of the $NaV_2(PO_4)_3$ (V-O ~ 1.91 Å), in line with the expected presence of vanadyl bonds.

Notably, the β-$VOPO_4$ reference material, featuring the shortest V=O bond length (~ 1.57 Å), exhibited the most significant shift towards higher emission energy among all compounds. The correlation between bond lengths and the presence of V=O, as illustrated in Figure S5, further supports this general observation. Clearly, a shorter V=O bond in the compound results in a significant shift towards higher emission energy of the $K\beta_{2,5}$ spectrum. Overall, our results confirm that the $K\beta_{2,5}$ features does not consistently provide descriptive information about the formal oxidation state despite a change in bonding also exists, but is mainly affected by the local structure. [24] Without a drastic difference in bond lengths, and a strong change in local symmetry, a mild transformation (Δ_E = ~0.82 eV), with respect to the relative position of the maximum peak, can only be observed as in the case of $Na_3V_2(PO_4)_3$ (V-O ~ 1.99 Å) and $NaV_2(PO_4)_3$ (V-O ~ 1.91 Å) with different formal oxidation state but closely similar structures (Figure 4a), compared to $KVPO_4F$ and $KVOPO_4$ (Δ_E = ~2.59 eV). The features strongly reflect the differences in the local geometric structure, and specifically the change in symmetry due to the distortion induced by shortened bond lengths in the presence of V=O.

Concerning the origin of the three features at the high energy $K\beta_{2,5}$ region, feature I decreases in intensity with the decrease of the fluorine content. Tentatively, this could therefore be related, at least in part, to the contribution of V-F bonds. This is also true for feature II wherein a possible mixed contributions from V-F and V-O bonds as they are also apparent for $KVPO_4F$ and $Na_3V_2(PO_4)_3$ and only a narrow difference between the spectra (Figure 4a) are observed despite having different coordination environments. The small variations in the fluoride and oxide 2*p* energies are anticipated to occur upon changes in bonding which explains the small difference given the similarities in bond lengths ($KVPO_4F$, V-O/F_{ave} ~ 1.98 Å; $Na_3V_2(PO_4)_3$, V-O_{ave} ~ 1.99 Å). In the series (Table S5a), since $KVPO_4F$ has the longest average bond lengths (~ 1.98 Å) and due to the ionicity of the V-F bonds, a reduced Coulombic attraction between the fluoride ions and the V^{3+} ions is expected to destabilize the fluoride 2*p* orbitals. This destabilization leads to transitions that are found at lower energy levels. To recall, there is a noticeable shift of the whole spectra toward higher emission energy for the case of $KVOPO_4$ since it contains V=O bonds (~ 1.67 Å) resulted in a stronger Coulombic attraction between oxide ions and V^{4+} ions leading to stabilized oxygen 2*p* orbitals and a more noticeable feature III. [35] Generally, the shift could be related to an increase in oxidation state of the vanadium [E_$NaV_2^{(IV)}(PO_4)_3$ - E_$Na_3V_2^{(III)}(PO_4)_3$ = ~ 0.82 eV], and/or to the presence of V=O in the compound series [E_$KV^{(IV)}OPO_4$ - E_$NaV_2^{(IV)}(PO_4)_3$ = ~ 2.03 eV], the latter having a much greater contribution, especially in the specific case of the given family of vanadyl-containing compounds. Feature III is highly affected by the increasing concentration of vanadyl-type oxygen, which is associated to the shortening of the bond length causing distortion in the local geometry and subsequently resulting in strong dipole effects influenced by the presence of π-bonding. These features are strongly affected by the V-F and V=O bond lengths, which are highly correlated to the degree of iono-covalency of the bonds that are evolving as expected in the series of materials (Figure S5b).

Assignment of the $K\beta_{2,5}$ emission line spectral features $KVPO_4F_{1-x}O_x$

Insights on the interpretation of the Kβ VtC features are obtained by *ab initio* modelling of the end member compounds $KVPO_4F$ and $KVOPO_4$. Distinguishing the different contributions or effects from the two inequivalent vanadium sites directly from the experimental spectra is not feasible, since only the global average signal of the two sites is recorded. However, using *ab initio* simulations, we could gain insight into their individual influences (Figure 5a and Figure 5b).

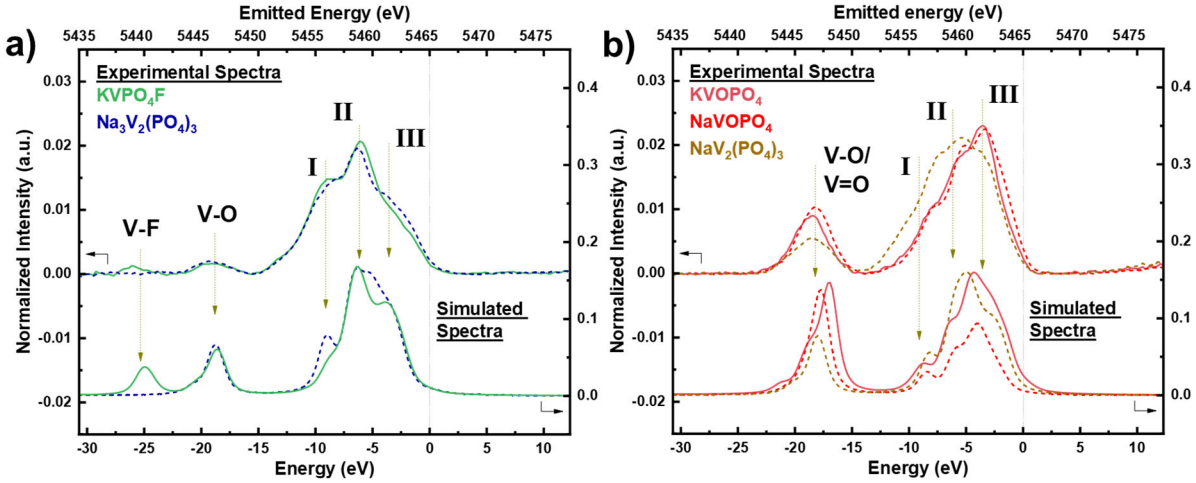

Figure 5. a) Experimental and simulated VtC Kβ XES spectra of $KVPO_4F$ along with $Na_3V_2(PO_4)_3$, and b) experimental and simulated VtC Kβ XES spectra of $KVOPO_4$ and along with $NaV_2(PO_4)_3$ and $NaVOPO_4$. The Na-based compounds are used as references.

In the Kβ" region, the results from the *ab initio* calculations confirm our peak assignments of the ligands and the types of bonding present, particularly V-F and V-O bonds (Figure 5a). Notably, for $KVPO_4F$, only a slight difference in the overall spectral feature is observed between the $V_{cis}O_4F_2$ and $V_{trans}O_4F_2$ octahedra, which mainly arises from the positions where the degeneracy of the occupied t_{2g} orbitals occurs (Figure S6a-b). This is reasonable considering that both octahedra are *quasi*-regular in terms of average bond lengths (~ 1.99 Å) as observed in all coordinations and the average difference between the bond lengths of all coordinated atoms is small (~ 0.03 Å). [6,36] This could also imply that the effective nuclear charge of vanadium does not change drastically in the two sites. On the other hand, for $KVOPO_4$, the V-O (~ 2.02 Å) and V=O (~ 1.67 Å) bonds are differentiated by their relative intensities, with V=O exhibiting a much stronger characteristic (Figure 5b). The difference in intensity is more apparent when compared with $NaV_2(PO_4)_3$ with only V-O (~ 1.91 Å) bond present. The existence of the short covalent vanadyl bond implies a reduction in the effective nuclear charge experienced by the oxo-ligands. This, in turn, leads to an increase in transition energy because the orbital energies are lowered. [35] Furthermore, the difference between the two vanadium sites is evident in the simulated spectra (Figure S7a-b). $\{V_{cis}{=}O\}O_5$ provides a higher contribution than $\{V_{trans}{=}O\}O_5$ to the intensity of the Kβ" region. The difference in contribution may come from the fact that for the V_{cis} environment, the coordination of the ligands can be fitted in EXAFS by a [5 + 1] coordination where as for the V_{trans} environment, it is [4 + 1 + 1] (four intermediate bonds, a long bond, and a short bond) [6].

In the $K\beta_{2,5}$ region, *ab initio* calculations also confirm that an increasing amount of vanadyl-type bonding leads to a shift in the spectra towards higher emission energy levels. This shift is primarily caused by the shortening of the V-X bond, which results in the mixing of predominantly vanadium 3*d*

orbitals with O 2*p* orbitals (Figure 6a-b). Vanadyl bonding is more covalent and introduces a geometrical distortion, lifting the degeneracy of the t_{2g} orbitals, with the d_{xy} orbital occupied by an unpaired d^1 electron. Strong π-bonding interactions between V d_{xz}, d_{yz} and filled O $2p_x$, $2p_y$ orbitals are also observed. [37]. Further differences appear when V=O bonding is present in alternating *cis*- and *trans*-configurations, as in the case in $KVOPO_4$. A complex mixing of orbitals can be observed for $\{V_{cis}{=}O\}O_5$ octahedra, whereas strong π-bonding interactions are evident for $\{V_{trans}{=}O\}O_5$ octahedra, particularly in the V *d*-DOS and O *p*-DOS where feature III is more pronounced and mainly contributed by the V_{trans} site (Figure S7a-b). These findings further support the notion that the increased intensity of the highest energy $K\beta_{2,5}$ region in $KVOPO_4$ indicates a stronger interaction with orbitals possessing an O 2*p* character which could be explained in the differences in coulombic attraction of the O^- anions and V^{4+} cation from V=O, and thus resulting in transitions shifted to higher energy. Further analysis of the results reveals that specific F and O *s*-DOS contribute to the intensity of feature I, which primarily originates from the combined contributions of the O *p*-DOS of the phosphate group together with the bridging ligand F/O 2*s** antibonding states. In general, for $KVPO_4F$, a mirrored characteristic is observed in the density of states (DOS) between the two different sites (*cis* and *trans*) and the coordinated ligands (Figure S6). For $KVOPO_4$ on the other hand, a complex density of state was simulated between the *cis* and *trans* sites, which could directly be connected to the varying bond lengths present in local geometry (Figure S7). Overall, a good reproduction of the experimental spectra is obtained using FDMNES, in spite of some limitations related to the structural complexity of the material. The simulated spectra at the Kβ" region confirm the experimental observation, with distinctly separated contributions from V-F and V-O at different emission energies, while V-O and V=O are differentiated in terms of difference in intensity. In the $K\beta_{2,5}$ region, the main identified features are preserved despite some mismatch between calculated and experimental intensities. It should also be noted that in the calculations, the E_F was arbitrarily set to reproduce the non-metallic character of the compounds.

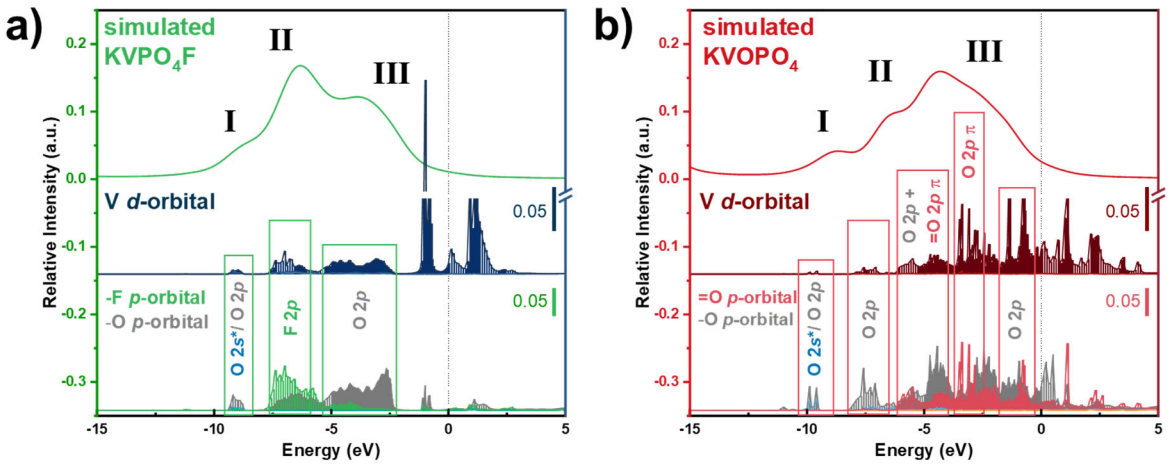

Figure 6. a-b) Simulated VtC Kβ XES of $KVPO_4F$ and $KVOPO_4$ and with their corresponding densities of states (DOS) at the $K\beta_{2,5}$ region, and c) the experimental spectra (open circles) along with the peak deconvolution (solid lines)

In summary, $K\beta_{2,5}$ VtC XES primarily reflects ligand-based molecular orbitals, with mixed *p* and *d* character around the V atoms. Contributions from 3*d* orbitals of V are negligible, and $K\beta_{2,5}$ VtC XES

corresponds to the *p*-projected electronic states, which was experimentally confirmed. Furthermore, the limited sensitivity of XES to core hole effects is due to the core hole being shielded by valence electrons of V in the unobserved 3*d* shell, leaving ligand orbitals relatively unaffected by changes in the effective nuclear charge of the V atom. Additionally, the minimal contribution of *d* orbitals of V in coordination complexes results in indirect sensitivity to changes in oxidation state but mainly more on to the metal-ligand distances. Only alterations in local geometry and the formation of new molecular orbitals significantly impact the spectrum.

Moreover, the comparison between the evolution of the VtC X-ray emission spectra of $KVPO_4F_{1-x}O_x$ pristine materials, with fine control of anion composition, offers an approach to understanding the electronic structures of these materials. This comparison potentially provides a key link in elucidating why these materials have such electrode potential as reported. [6,38] Here, we delve into a broad comprehension of the electronic structure in correlation with the materials' crystal chemistry, and this understanding marks an essential step towards comprehending and controlling electrochemical properties and performance. Ultimately, further studies on the (de)intercalated phases are needed to be fully explored to realize the crucial link.

CONCLUSION

This paper demonstrates that VtC Kβ XES is a powerful tool to describe the occupied electronic states close to the Fermi level, which play a crucial role in the redox processes and govern the electrochemical properties of the materials functioning as positive electrodes for KIBs. Our critical insights on the electronic properties of the series of pristine materials is crucial in understanding the electrochemical mechanisms involved once they are employed as electrode materials. The technique's high sensitivity to chemical bonding characteristics allows for the discrimination of light anions such as F^- and O^{2-}, which are virtually impossible to distinguish using routine bulk techniques such as XAS. Moreover, the use of high-energy incident X-rays in VtC Kβ XES measurements overcomes the conventional limitations of soft X-ray spectroscopies, enabling a comprehensive analysis of the bulk properties of the materials and allowing its potential applicability to perform *operando* measurements.

By adopting a systematic approach combining experimental VtC Kβ XES spectra with *ab initio* calculations, we achieved a comprehensive understanding of the electronic structure near the Fermi level and its evolution, particularly in the presence of a highly covalent V=O bond. Additionally, leveraging our prior knowledge on the crystallographic information of the materials enabled us to conduct a robust analysis and interpretation of the complex nature of the electronic structure, especially in compounds containing (or not) covalent vanadyl-type environments. The synergy between experimental data and theoretical modelling provides valuable insights into the electronic behavior of these materials, shedding light on their high applicability to solid state systems more specifically to electrode materials in metal-ion batteries.

ACKNOWLEDGMENTS

As part of the DESTINY PhD Programme, the authors acknowledge funding from the European Union's Horizon2020 research and innovation programme under the Marie Skłodowska-Curie Actions COFUND (Grant Agreement #945357). Funding from the Synchrotron SOLEIL is also recognized.

ANR is acknowledged for funding the RS2E network through the STORE-EX Labex Project ANR- 10-LABX-76-01, and the ANR TROPIC project ANR-CE05-0026. The authors also acknowledge the European Synchrotron Radiation Facility (ESRF) for providing beamtime at the BM16 (Proposal No. CH6103) and ID20 beamline (Proposal No. CH6327). Dr. Phuong Nam Le Pham is gratefully appreciated for technical support during the beamtimes. Dr. Felisa Berenguer (Synchrotron SOLEIL) and Prof. Dany Carlier (ICMCB) are also thanked for fruitful discussions and advice throughout this work.

REFERENCES

[1] Y. Xu, M. Titirici, J. Chen, F. Cora, P.L. Cullen, J.S. Edge, K. Fan, L. Fan, J. Feng, T. Hosaka, J. Hu, W. Huang, T.I. Hyde, S. Imtiaz, F. Kang, T. Kennedy, E.J. Kim, S. Komaba, L. Lander, P.N. Le Pham, P. Liu, B. Lu, F. Meng, D. Mitlin, L. Monconduit, R.G. Palgrave, L. Qin, K.M. Ryan, G. Sankar, D.O. Scanlon, T. Shi, L. Stievano, H.R. Tinker, C. Wang, H. Wang, H. Wang, Y. Wu, D. Zhai, Q. Zhang, M. Zhou, J. Zou, 2023 roadmap for potassium-ion batteries, J. Phys. Energy. 5 (2023) 021502. https://doi.org/10.1088/2515-7655/acbf76.

[2] Z. Jian, W. Luo, X. Ji, Carbon Electrodes for K-Ion Batteries, J. Am. Chem. Soc. 137 (2015) 11566–11569. https://doi.org/10.1021/jacs.5b06809.

[3] K. Kubota, M. Dahbi, T. Hosaka, S. Kumakura, S. Komaba, Towards K-Ion and Na-Ion Batteries as "Beyond Li-Ion," Chem. Rec. 18 (2018) 459–479. https://doi.org/10.1002/tcr.201700057.

[4] K. Chihara, A. Katogi, K. Kubota, S. Komaba, KVPO4F and KVOPO4 toward 4 volt-class potassium-ion batteries, Chem. Commun. 53 (2017) 5208–5211. https://doi.org/10.1039/c6cc10280h.

[5] T. Broux, T. Bamine, F. Fauth, L. Simonelli, W. Olszewski, C. Marini, M. Ménétrier, D. Carlier, C. Masquelier, L. Croguennec, Strong Impact of the Oxygen Content in Na3V2(PO4)2F3-yOy ($0 \leq y \leq 2$) on Its Structural and Electrochemical Properties, Chem. Mater. 28 (2016) 7683–7692. https://doi.org/10.1021/acs.chemmater.6b02659.

[6] R. Wernert, L.H.B. Nguyen, E. Petit, P.S. Camacho, A. Iadecola, A. Longo, F. Fauth, L. Stievano, L. Monconduit, D. Carlier, L. Croguennec, Controlling the Cathodic Potential of KVPO 4 F through Oxygen Substitution, Chem. Mater. 34 (2022) 4523–4535. https://doi.org/10.1021/acs.chemmater.2c00295.

[7] E. Boivin, R. David, J.-N. Chotard, T. Bamine, A. Iadecola, L. Bourgeois, E. Suard, F. Fauth, D. Carlier, C. Masquelier, L. Croguennec, LiVPO4F1- yOy Tavorite-Type Compositions: Influence of the Concentration of Vanadyl-Type Defects on the Structure and Electrochemical Performance, Chem. Mater. 30 (2018) 5682–5693. https://doi.org/10.1021/acs.chemmater.8b02138.

[8] E. Boivin, A. Iadecola, F. Fauth, J.-N. Chotard, C. Masquelier, L. Croguennec, Redox Paradox of Vanadium in Tavorite LiVPO4F1-yOy, Chem. Mater. 31 (2019) 7367–7376. https://doi.org/10.1021/acs.chemmater.9b01987.

[9] M. Bianchini, J.M. Ateba Mba, P. Dagault, E. Bogdan, D. Carlier, E. Suard, C. Masquelier, L. Croguennec, Multiple phases in the ε-VPO4O-LiVPO4O-Li 2VPO4O system: A combined solid state electrochemistry and diffraction structural study, J. Mater. Chem. A. 2 (2014) 10182–10192. https://doi.org/10.1039/c4ta01518e.

[10] M. Bianchini, F. Fauth, N. Brisset, F. Weill, E. Suard, C. Masquelier, L. Croguennec, Comprehensive investigation of the Na3V2(PO4)2F3-NaV2(PO4)2F3 system by operando high resolution synchrotron X-ray diffraction, Chem. Mater. 27 (2015) 3009–3020. https://doi.org/10.1021/acs.chemmater.5b00361.

[11] L.H.B. Nguyen, A. Iadecola, S. Belin, J. Olchowka, C. Masquelier, D. Carlier, L. Croguennec, A combined operando synchrotron x-ray absorption spectroscopy and first-principles density functional theory study to unravel the vanadium redox paradox in the Na3V2(PO4)2F3−Na3V2(PO4)2FO2 compositions, J. Phys. Chem. C. 124 (2020) 23511–23522. https://doi.org/10.1021/acs.jpcc.0c06967.

[12] K.H. Lii, C.H. Li, T.M. Chen, S.L. Wang, Synthesis and structural characterization of sodium vanadyl(IV) orthophosphate NaVOPO4, Zeitschrift Fur Krist. - New Cryst. Struct. 197 (1991) 67–73. https://doi.org/10.1524/zkri.1991.197.1-2.67.

[13] A.M. Abakumov, S.S. Fedotov, E. V. Antipov, J.-M. Tarascon, Solid state chemistry for developing better metal-ion batteries, Nat. Commun. 11 (2020) 1–14. https://doi.org/10.1038/s41467-020-18736-7.

[14] M. Fehse, A. Iadecola, L. Simonelli, A. Longo, L. Stievano, The rise of X-ray spectroscopies for unveiling the functional mechanisms in batteries, Phys. Chem. Chem. Phys. 23 (2021)

23445–23465. https://doi.org/10.1039/d1cp03263a.
[15] R. Wernert, A. Iadecola, L. Stievano, D. Carlier, L. Croguennec, Origin of Vanadium Site Sequential Oxidation in K x VPO 4 F 1– y O y, Chem. Mater. 35 (2023) 617–627. https://doi.org/10.1021/acs.chemmater.2c03132.
[16] A. Longo, R. Wernert, A. Iadecola, C.J. Sahle, L. Stievano, L. Croguennec, D. Carlier, A. Mirone, An Original Empirical Method for Simulating V L 2,3 Edges: The Example of KVPO 4 F and KVOPO 4 Cathode Materials, J. Phys. Chem. C. 126 (2022) 19782–19791. https://doi.org/10.1021/acs.jpcc.2c05334.
[17] L.H.B. Nguyen, T. Broux, P.S. Camacho, D. Denux, L. Bourgeois, S. Belin, A. Iadecola, F. Fauth, D. Carlier, J. Olchowka, C. Masquelier, L. Croguennec, Stability in water and electrochemical properties of the Na3V2(PO4)2F3 – Na3(VO)2(PO4)2F solid solution, Energy Storage Mater. 20 (2019) 324–334. https://doi.org/10.1016/j.ensm.2019.04.010.
[18] M. Rovezzi, P. Glatzel, Hard x-ray emission spectroscopy: A powerful tool for the characterization of magnetic semiconductors, Semicond. Sci. Technol. 29 (2014). https://doi.org/10.1088/0268-1242/29/2/023002.
[19] E. Gallo, P. Glatzel, Valence to core X-ray emission spectroscopy, Adv. Mater. 26 (2014) 7730–7746. https://doi.org/10.1002/adma.201304994.
[20] G. Hölzer, M. Fritsch, M. Deutsch, J. Härtwig, E. Förster, Kα1,2 and Kβ1,3 x-ray emission lines of the 3d transition metals, Phys. Rev. A - At. Mol. Opt. Phys. 56 (1997) 4554–4568. https://doi.org/10.1103/PhysRevA.56.4554.
[21] S.D. Gamblin, D.S. Urch, Metal Kβ X-ray emission spectra of first row transition metal compounds, J. Electron Spectros. Relat. Phenomena. 113 (2001) 179–192. https://doi.org/10.1016/S0368-2048(00)00416-3.
[22] E.P. Jahrman, W.M. Holden, N. Govind, J.J. Kas, J. Rana, L.F.J. Piper, C. Siu, M.S. Whittingham, T.T. Fister, G.T. Seidler, Valence-to-core X-ray emission spectroscopy of vanadium oxide and lithiated vanadyl phosphate materials, J. Mater. Chem. A. 8 (2020) 16332–16344. https://doi.org/10.1039/d0ta03620j.
[23] J.B. Jones, D.S. Urch, Metal-ligand bonding in some vanadium compounds: A study based on X-ray emission data, J. Chem. Soc. Dalt. Trans. (1975) 1885–1889. https://doi.org/10.1039/DT9750001885.
[24] G. Smolentsev, A. V Soldatov, J. Messinger, K. Merz, T. Weyhermüller, U. Bergmann, Y. Pushkar, J. Yano, V.K. Yachandra, P. Glatzel, X-ray emission spectroscopy to study ligand valence orbitals in Mn coordination complexes, J. Am. Chem. Soc. 131 (2009) 13161–13167. https://doi.org/10.1021/ja808526m.
[25] C.J. Pollock, K.M. Lancaster, K.D. Finkelstein, S. Debeer, Study of iron dimers reveals angular dependence of valence-to-core X-ray emission spectra, Inorg. Chem. 53 (2014) 10378–10385. https://doi.org/10.1021/ic501462y.
[26] C.J. Pollock, S. DeBeer, Insights into the Geometric and Electronic Structure of Transition Metal Centers from Valence-to-Core X-ray Emission Spectroscopy, Acc. Chem. Res. 48 (2015) 2967–2975. https://doi.org/10.1021/acs.accounts.5b00309.
[27] O. Proux, E. Lahera, W. Del Net, I. Kieffer, M. Rovezzi, D. Testemale, M. Irar, S. Thomas, A. Aguilar-Tapia, E.F. Bazarkina, A. Prat, M. Tella, M. Auffan, J. Rose, J.-L. Hazemann, High-Energy Resolution Fluorescence Detected X-Ray Absorption Spectroscopy: A Powerful New Structural Tool in Environmental Biogeochemistry Sciences, J. Environ. Qual. 46 (2017) 1146–1157. https://doi.org/10.2134/jeq2017.01.0023.
[28] C.J. Sahle, F. Gerbon, C. Henriquet, R. Verbeni, B. Detlefs, A. Longo, A. Mirone, M.C. Lagier, F. Otte, G. Spiekermann, S. Petitgirard, K. Kvashnina, A compact von Hámos spectrometer for parallel X-ray Raman scattering and X-ray emission spectroscopy at ID20 of the European Synchrotron Radiation Facility, J. Synchrotron Radiat. 30 (2023) 251–257. https://doi.org/10.1107/S1600577522011171.
[29] V.A. Solé, E. Papillon, M. Cotte, P. Walter, J. Susini, A multiplatform code for the analysis of energy-dispersive X-ray fluorescence spectra, Spectrochim. Acta - Part B At. Spectrosc. 62 (2007) 63–68. https://doi.org/10.1016/j.sab.2006.12.002.
[30] M. Wojdyr, Fityk: A general-purpose peak fitting program, J. Appl. Crystallogr. 43 (2010) 1126–1128. https://doi.org/10.1107/S0021889810030499.

[31] O. Bunău, A.Y. Ramos, Y. Joly, The FDMNES code, in: 2021: pp. 1–6. https://doi.org/10.1107/S1574870720003304.
[32] Y. Joly, A.Y. Ramos, O. Bunău, Finite-difference method for the calculation of X-ray spectroscopies, in: 2022: pp. 1–7. https://doi.org/10.1107/s1574870722001598.
[33] O. Bunău, Y. Joly, Self-consistent aspects of x-ray absorption calculations, J. Phys. Condens. Matter. 21 (2009) 345501. https://doi.org/10.1088/0953-8984/21/34/345501.
[34] S. Park, Z. Wang, Z. Deng, I. Moog, P. Canepa, F. Fauth, D. Carlier, L. Croguennec, C. Masquelier, J.-N. Chotard, Crystal Structure of Na2V2(PO4)3, an Intriguing Phase Spotted in the Na3V2(PO4)3-Na1V2(PO4)3System, Chem. Mater. 34 (2022) 451–462. https://doi.org/10.1021/acs.chemmater.1c04033.
[35] J.A. Rees, A. Wandzilak, D. Maganas, N.I.C. Wurster, S. Hugenbruch, J.K. Kowalska, C.J. Pollock, F.A. Lima, K.D. Finkelstein, S. DeBeer, Experimental and theoretical correlations between vanadium K-edge X-ray absorption and K β emission spectra, J. Biol. Inorg. Chem. 21 (2016) 793–805. https://doi.org/10.1007/s00775-016-1358-7.
[36] R. Wernert, L.H.B. Nguyen, A. Iadecola, F. Weill, F. Fauth, L. Monconduit, D. Carlier, L. Croguennec, Self-Discharge Mechanism of High-Voltage KVPO 4 F for K-Ion Batteries, ACS Appl. Energy Mater. 5 (2022) 14913–14921. https://doi.org/10.1021/acsaem.2c02379.
[37] C.J. Ballhausen, H.B. Gray, The Electronic Structure of the Vanadyl Ion, Inorg. Chem. 1 (1962) 111–122. https://doi.org/10.1021/ic50001a022.
[38] R. Wernert, L.H.B. Nguyen, D. Carlier, L. Croguennec, Mixed anion chemistry as a way to tune the electrochemical properties of vanadium oxyfluoride phosphates in alkali-ion batteries, Solid State Sci. 146 (2023) 107358. https://doi.org/10.1016/j.solidstatesciences.2023.107358.

GRAPHICAL ABSTRACT